

1 **Off-fault Seismicity Suggests Deep Creep on the Northern San Jacinto Fault**

2 **M. L. Cooke¹ and J. L. Beyer¹**

3 ¹Geosciences Department, University of Massachusetts – Amherst, USA

4 Corresponding author: Michele Cooke (cooke@geo.umass.edu)

5 **Key Points:**

- 6 • Crustal deformation models demonstrate the plausibility of deep creep along the
7 northern San Jacinto fault to account for nearby enigmatic normal slip mechanisms
- 8 • Microseismicity that records off-fault deformation may record stresses that differ from
9 interseismic loading of the primary fault surfaces
- 10 • Where faults exhibit creep at any crustal level, caution should be used in the inversion
11 of nearby focal mechanisms for interseismic fault loading

12

13 **Abstract**

14 Within the San Bernardino basin, focal mechanisms show normal slip events that are inconsistent
15 with the interseismic strike-slip loading of the nearby San Jacinto and San Andreas faults. The
16 discrepancy may owe to deep (> 10 km depth), creep along the northern San Jacinto fault. The
17 enigmatic normal slip events occur to the northeast of the fault and primarily below 10 km depth,
18 consistent with off-fault deformation due to spatially non-uniform deep creep rates. Consequently,
19 if these normal slip events are included in stress inversions from the seismic catalog, the results
20 may provide inaccurate information about fault loading. Here, we show that models with deep
21 creep on the northern San Jacinto fault that match first-order pattern of observed normal slip focal
22 mechanisms in the basin and that this deep creep cannot be detected with GPS data due to the
23 proximity of the San Andreas fault.

24 **Plain Language Summary**

25 Over the past 36 years, seismic stations have recorded the style of deformation from thousands of
26 small earthquakes in the San Bernardino basin, California. Within this basin, many earthquakes
27 below 7.5 depth show deformation that doesn't match what we expect for this region during the
28 current period between large damaging earthquakes along the San Jacinto and San Andreas
29 faults. Rather than showing expected horizontal slip, many of these earthquakes show vertical
30 movement. We use crustal deformation models to show that vertical movement can be produced
31 in the basin if the northern portion of the San Jacinto fault creeps at depth; this portion of the
32 fault is constantly moving rather than locked, like the San Andreas. Traditional GPS-based
33 approaches to detect deep creep don't work here because the faults are too close to one another.
34 The findings of this study demonstrate that small earthquakes that occur adjacent to and between
35 faults can have very different style of deformation than the large ground rupturing earthquakes
36 produced along active faults. This means that scientists should not use the information recorded
37 by these small earthquakes in the San Bernardino basin to predict loading of the San Andreas and
38 San Jacinto faults.

39 **1 Introduction**

40 The assumption built into seismic hazard assessments, such as Unified California
41 Earthquake Rupture Forecast (Field et al., 2014), is that the seismic catalog collected over the
42 past several decades accurately represents the loading of active faults within California. This
43 assumption is challenged by the limited duration of the seismic catalog compared to the 100-
44 1000 year recurrence intervals along most faults within California. For example, during the
45 recording of the seismic catalog, the San Andreas fault (SAF) south of Cajon Pass has had fewer
46 earthquakes than smaller nearby faults (e.g. Yang et al., 2012). Although this fault has the
47 greatest potential for large earthquakes in southern California (e.g. Field et al., 2014), it is
48 relatively under-sampled within the seismic catalog. Furthermore, small earthquakes in the crust
49 may record off-fault deformation rather than slip along the primary slip planes of active faults
50 (Cheng et al., 2018). Where off fault deformation differs from loading of the primary faults, the
51 stress state inferred from microseismicity may not accurately reflect the interseismic loading of
52 the major active faults capable of producing ground rupturing earthquakes.

53 While we might expect the focal mechanisms from recorded microseismicity along the
54 southern SAF system to reveal that dextral deformation dominates this system, Yang et al. (2012)
55 show that some regions, such as the San Bernardino basin, produce predominantly normal-slip
56 events (Fig. 1a). These focal mechanisms contrast the observations of long-term strike-slip along
57 the nearby SAF (e.g. McGill et al., 2013; McGill et al., 2015) and San Jacinto fault (SJf) (e.g.
58 Anderson et al., 2004; Onderdonk et al., 2015). The normal slip focal mechanisms also disagree
59 with crustal deformation models of the region that show dextral interseismic loading (e.g.
60 Johnson, 2013; Fig. 1b; Loveless and Meade, 2011; Smith-Konter et al., 2011). This discrepancy
61 suggests that the seismicity in the San Bernardino basin is not consistent with the loading of the
62 SAF and SJf flanking the basin.

63 Some of the normal slip events that occur just to the northeast of the northern San Jacinto
64 fault, have been associated with secondary normal faults revealed by geophysical imaging of the
65 top of basement (Anderson et al., 2004). Small normal faults trend sub-parallel to the SJf and
66 bound the edges of a local basement low that developed where the SJf changes strike (Fig. 1c).
67 While co-seismic slip along the SJf could promote extension of this basin, the production of
68 normal slip earthquakes during the interseismic period when these faults are presumed to be
69 locked throughout the seismogenic crust remains enigmatic. Furthermore, the occurrence of
70 normal slip earthquakes extends beyond the geophysically imaged extensional basin. The San
71 Bernardino basin is expected to have dextral loading between large earthquake events on the SAF
72 and SJf (Fig. 1b).

73 Slip gradients along strike-slip faults, such as near the tips of earthquake ruptures, can
74 produce off-fault stresses and subsequent aftershocks that differ from the loading of the faults
75 (e.g. Hardebeck, 2014; Oppenheimer, 1990). Yang et al. (2012) report temporary changes in
76 focal mechanism slip sense after large magnitude earthquakes in southern California. Cheng et
77 al. (2018) report off-fault aftershocks that have distinct slip sense from the events that occur
78 along the Anza segment of the San Jacinto fault, to the south of the study area of this study.
79 Because the San Bernardino basin has not experienced a large event during the catalog record,
80 we propose that spatially non-uniform creep at depth along the northern SJf may drive the
81 observed normal slip microseismicity in the San Bernardino basin. Consequently, the
82 microseismicity in our multi-decadal catalog may record both interseismic dextral loading of the
83 region as well as off-fault deformation associated with deep creep on the northern SJf. We use
84 crustal deformation models to show the potential for slip to produce off-fault microseismicity
85 that obfuscates our interpretation of fault loading from the seismic catalog.

86 2. Methods

87 2.1 Reliable catalog of focal mechanisms in the San Bernardino basin

88 We analyze the three-dimensional distribution of focal mechanisms in the San
89 Bernardino basin to assess the spatial pattern of the enigmatic normal slip events. A catalog of
90 relocated southern California focal mechanisms from January 1981 through September 2016 are

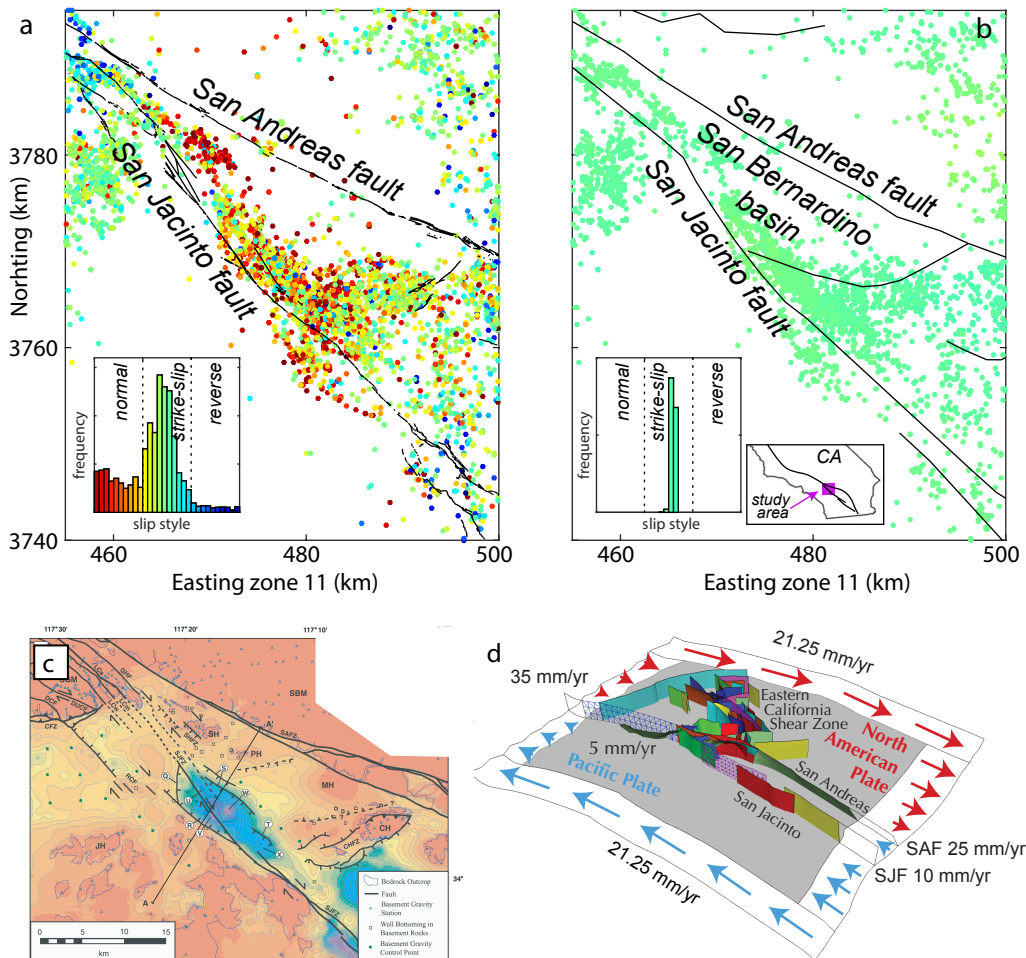


Figure 1. a) High quality focal mechanisms (nodal plane uncertainty $< 45^\circ$) from 1981 through September of 2016 in the relocated catalog of (Hauksson et al., 2012) with traces of faults active within the last 15 ka (USGS & CGS, 2006). Colors show slip sense with tangent of slip rake scaled to the 0-3 range of $A\phi$ slip sense (Simpson, 1997). b) Slip sense predicted by interseismic crustal deformation model of D at locations of the seismic events recorded in the catalog. Traces of modeled faults shown in black. Insets show histograms of slip sense. The normal slip events within the San Bernardino basin are not expected from loading between large earthquakes. c) Basement depth inverted from gravity data shows secondary normal faults that flank the San Jacinto fault (taken from Anderson et al., 2004). The normal slip focal mechanisms extend beyond the interpreted graben. d) Model of 63 active faults in the region used to build the steady state and interseismic models of crustal deformation. The lateral edges of the horizontal crack are loaded with plate velocities to simulate the regional tectonic loading (taken from Beyer et al., in revision).

91 available from the Southern California Earthquake Center database (Hauksson et al., 2012). We
92 limit the analysis to high-quality events, with nodal plane uncertainty $< 45^\circ$ (Yang et al., 2012).
93 Figure 2a shows the 6081 high-quality events between Easting 455000 and 500000 meters UTM
94 zone 11 and Northing 3740000 and 3795000 meters. In this region, the mean slip sense assessed
95 with a 600-event moving window remains around $A\phi = 1.2$ during the time period of the catalog,
96 indicating overall normal and strike-slip events (black line on Fig. 2a).

97 Excluding earthquakes smaller than the magnitude completeness limit eliminates bias of
98 including small events that are recorded because they occur close to seismic instruments. The
99 completeness limit of the San Bernardino basin seismic catalog improves with time as seismic
100 stations are added to the network. We calculate the evolving magnitude completeness limit using
101 the maximum curvature method (Wiemer and Wyss, 2000) for a moving window of 600 events
102 advanced in increments of 100 events. The magnitude completeness improves around 2002 and
103 2012 so that we can define three epochs of magnitude completeness limits (red line on Fig. 2b).
104 To determine a reliable catalog of events that exceed completeness, we exclude earthquakes
105 smaller than M2 for epoch1 (1981 – 2001), smaller than M1.5 for epoch2 (2002-2011), and
106 smaller than M1.0 for epoch3 (2012 – September 2016). The resulting catalog of 3920 reliable
107 events shows consistent slip sense ($A\phi = 1.2$) throughout the 36-year catalog, suggesting that the
108 catalog is not significantly impacted by transient changes, such as stress changes from nearby
109 large earthquakes or anomalous periods of enhanced normal faulting (Fig. 2c).

110 2.2 Steady-state and interseismic crustal models of the region

111 To simulate the stresses in the San Bernardino basin that drive interseismic
112 microseismicity, we have developed 3D Boundary Element Method stressing rate models that
113 simulate interseismic loading between earthquakes using a two-step approach. For the first step,
114 multiple earthquake cycles are simulated in a steady-state model where all portions of the fault
115 surfaces slip. The second step of the approach implements a back-slip approach to simulate the
116 interseismic loading of the faults, where the slip distribution from the steady-state model is applied
117 to faults below the locking depth (e.g. Marshall et al., 2009).

118 For the first stage of interseismic model development, we produce a steady-state model of
119 crustal deformation over many earthquake cycles. The model incorporates active faults surfaces
120 of the region based on the SCEC Community Fault Model v. 4.0 and re-meshed for more
121 uniform triangular element size and coincident nodes along fault intersections (Fig. 1d). The
122 fault geometry used in this study follows that of the preferred model of Beyer et al. (in revision)
123 with revised resolution of the San Jacinto fault (average element length ~ 2.6 km). Within the 3D
124 models, faults are extended to 35 km depth, where they merge with a horizontal crack.
125 Deformation along this crack simulates distributed deformation below the seismogenic crust.
126 Following Beyer et al. (in revision) this study applies a plate tectonic movement equivalent to
127 47.5 mm/yr at 322.5° (e.g. DeMets et al., 2010) to the sides of the model that parallel plate
128 velocity and a velocity gradient along the sides of the model perpendicular to plate velocity.
129 Where faults meet the lateral edges of the model, the applied velocity has a step and

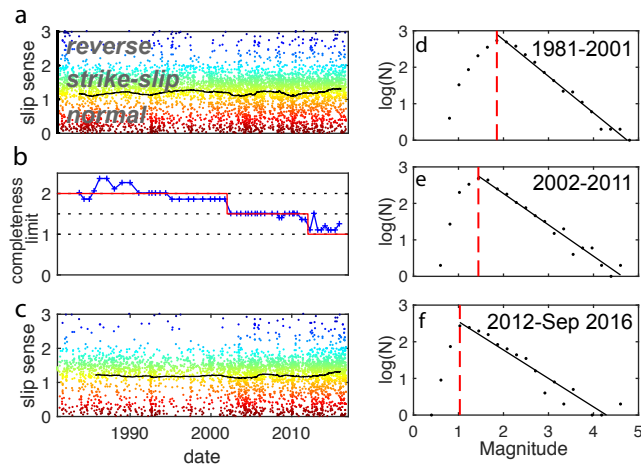


Figure 2. a) Focal mechanisms from Hauksson et al. (2012) within the region of Figure 1. The average slip sense for moving window of 600 events shown with black line. Warm colors are normal events, cool colors are reverse events, and green are strike-slip events. b) Magnitude completeness limit for a moving window of 600 events advanced in 100 event increments shown in blue. The stepped red line shows the three stages of magnitude completeness during the record. c) The 3920 events that exceed the three-phased magnitude completeness limit have mean $A\phi$ of 1.2 ± 0.04 , indicating limited variation in slip sense during the record. (d-e) The log of frequency demonstrates the completeness of the catalog for each epoch: 1981 through 2001 (d), 2002 through 2011 (e) and after 2012 (f). The completeness limit (red dashed line) decreases in each successive epoch.

130 corresponding slip rates are applied to the endmost patch of the fault to avoid slip rates going to
131 zero at these artificial fault tips (Fig. 4a). The shear traction-free faults in the center of the model
132 slip in response to tectonic loading and interaction with each other. This low shear traction
133 simulates dynamic conditions when most of the fault slip occurs.

134 To simulate interseismic loading between large earthquakes, the interseismic models
135 apply slip rates from the long-term model below a prescribed locking depth. Using this
136 approach, these interseismic models can simulate deep creep. To avoid a sharp step between
137 slipping and locked regions, fault elements within a 2.5 km high transitional band above the
138 locking depth are prescribed 50% of the slip rate values of the long-term model. We explore the
139 impact of varying locking depth from 7.5 to 20 km along the San Jacinto fault while all other
140 faults have a 20 km locking depth. In all the models, stress tensors are sampled at points in the
141 model corresponding to the locations of reliable focal mechanisms. This allows the model results
142 to be directly compared to the observed seismicity.

143 **3. Focal mechanism distribution supports deep creep along the northern San Jacinto fault**

144 Three aspects of the three-dimensional distribution of interseismic events in the San
145 Bernardino basin are consistent with deep creep along the northern SJF. Firstly, the contrast of
146 high rate of microseismicity along the SJF compared to the quiet nearby SAF (Fig. 3a).
147 Observations of abundant microseismicity adjacent to creeping faults (e.g. Harris, 2017) support
148 the inference that the SJF could have active creep whereas the SAF is currently locked.
149 Secondly, projecting the focal mechanisms of the reliable catalog into a north-south profile
150 reveals that most of the enigmatic normal slip events of the San Bernardino basin occur below
151 ~ 7.5 km depth (Fig. 3b). If the creep is contributing to the off-fault normal slip microseismicity,
152 then the fault below this depth may be creeping. Along the Anza section of the San Jacinto fault,
153 south of this study area, normal slip microseismicity also occurs near the SJF at depths of 10-13
154 km (Cheng et al., 2018). The discrepancy between locking depth of the Anza section of the SJF
155 and base of seismicity have led to inference of creep below 10 km along this section of the SJF
156 (Wdowinski, 2009), consistent with the depths of off-fault normal microseismicity.

157 The third aspect of the focal mechanism distribution that supports deep creep is that the
158 normal slip focal mechanisms are primarily located northeast, and not southwest, of the SJF (Fig.
159 3a). This pattern is consistent with the results of steady-state crustal deformation models of the
160 region that simulate deformation over multiple earthquake cycles (Resor et al., 2018; Fig. 4b).
161 This model shows a southward increasing dextral slip rate along the northern San Jacinto fault
162 that produces a region of positive dilation (increased mean normal tension) within the San
163 Bernardino basin. This long-term dilation can promote normal slip events by unclamping
164 potential slip surfaces relative to those outside of the basin. The location of off-fault dilation
165 correlates to the location of slip rate gradient along the SJF (Fig. 4b). Consequently, deep dilation
166 consistent with the occurrence of normal slip events below ~ 7.5 km in the San Bernardino basin
167 may be associated with creep along the SJF below ~ 7.5 km. Taken together, the three-

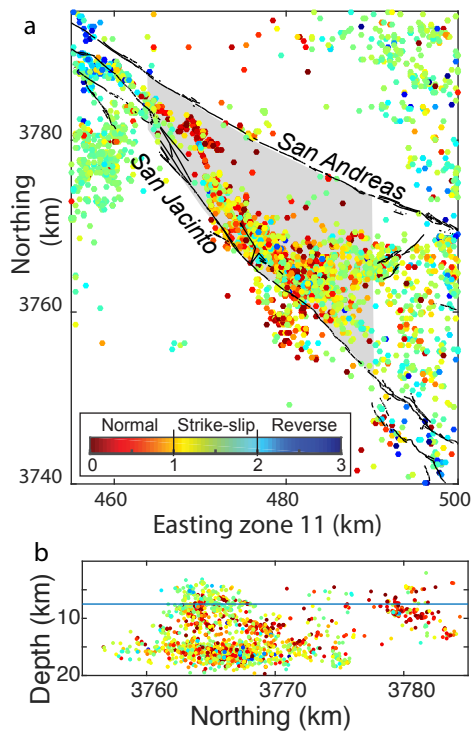


Figure 3. a) Map view of reliable focal mechanisms that pass the completeness test colored by slip sense. Enigmatic normal slip events occur within the San Bernardino basin, between the San Andreas and San Jacinto faults. Dashed fault traces are the graben bounding normal faults imaged by Anderson (2004) in Fig. 1C. b) Focal mechanisms of the San Bernardino basin (grey region of a) projected into a N-S profile. Slip sense color same as in a. The normal slip focal mechanisms within the San Bernardino basin occur predominantly below 7.5 km depth

168 dimensional distribution of focal mechanisms within the San Bernardino basin is consistent with
169 southward increasing creep rate along the northern SJF at depth.

170 **4. Simulating deep creep on the northern San Jacinto fault**

171 To investigate the impact of deep interseismic creep on the northern San Jacinto fault, we
172 investigate the sensitivity of focal mechanism slip sense within the San Bernardino basin to
173 locking depth along the northern SJf (San Bernardino and San Jacinto Valley segments). The
174 interseismic models apply 20 km locking depth on all other faults, consistent with the general
175 base of seismicity of the region (e.g. Yang et al., 2012). The overall slip sense of
176 microseismicity within the San Bernardino basin (grey region in Fig. 5a) is best matched by
177 interseismic models with locking depth < 12.5 km along the northern SJF (Fig. 5b). Results for
178 locking depths of 7.5 and 10 km show similar fit within 1σ . The interseismic model with 10 km
179 locking depth produces normal slip events that are spatially consistent with the observed
180 enigmatic normal slip focal mechanisms within the San Bernardino basin (Fig. 5a). The normal
181 slip events in the interseismic model occur to the northeast of the San Jacinto fault near the
182 gradient in dextral slip rate along the fault.

183 While creep below 10-13 km has been inferred along the southern San Jacinto fault from
184 geodetic evidence of shallow locking depths (Fialko, 2006; Smith-Konter et al., 2011;
185 Wdowinski, 2009), geodetic inversions for the northern San Jacinto fault suggest a deep (~ 20
186 km) locking depth (Smith-Konter et al., 2011). Because the San Jacinto and San Andreas faults
187 approach within 10 km of each other at the San Bernardino basin, the inversions of geodetic data
188 for locking depth in this region may not distinguish the independent locking depths of the SJf
189 and SAf. To explore this, we compare the interseismic velocities at GPS sties from two models:
190 one that has 15 km locking depth on all faults and another that has 10 km locking depth on the
191 northern SJf and 20 km on all other faults. The station velocities from the two models cannot be
192 distinguished from the observed GPS station velocities determined by Herbert et al. (2014) (Fig.
193 5c). Consequently, geodetic data cannot eliminate deep creep on the northern San Jacinto fault as
194 a potential mechanism for the off-fault normal slip microseismicity within the San Bernardino
195 basin.

196 **5. Discussion**

197 Some differences in the predicted interseismic slip sense at locations of microseismicity
198 and observed slip sense reveal aspects of the model that may not adequately capture the 3D
199 complexity of active deformation along the San Jacinto fault. Within the model, normal slip
200 microseismicity occurs within a narrow band adjacent to the SJf with strike-slip and reverse events
201 outside of this band where the catalog records a combination of normal and strike-slip focal
202 mechanisms. The nature of fault surface discretization within the model leads to artificially linear
203 and abrupt transitions from slipping to transitional ($1/2$ long term slip rate) to locked portions of
204 the fault. These abrupt transitions may produce a more localized pattern of normal slip
205 microseismicity than observed. Furthermore, the model does not consider host rock

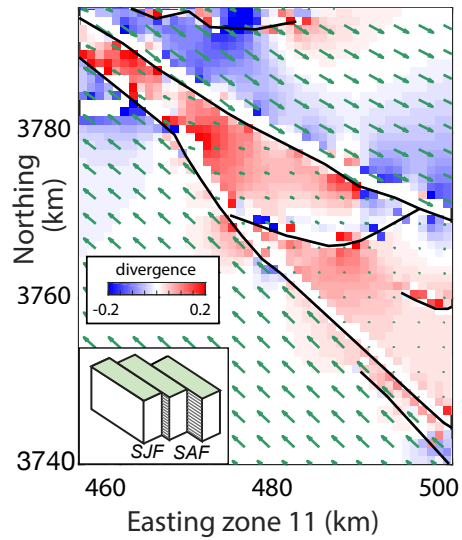


Figure 4. Green arrows show the velocities from the steady state model that simulates many earthquake cycles. The divergence of this velocity field reveals regions of overall contraction (negative dilation blue) and extension (positive dilation red) due to slip distribution along the faults. Inset cartoon shows the set-up of the steady-state model.

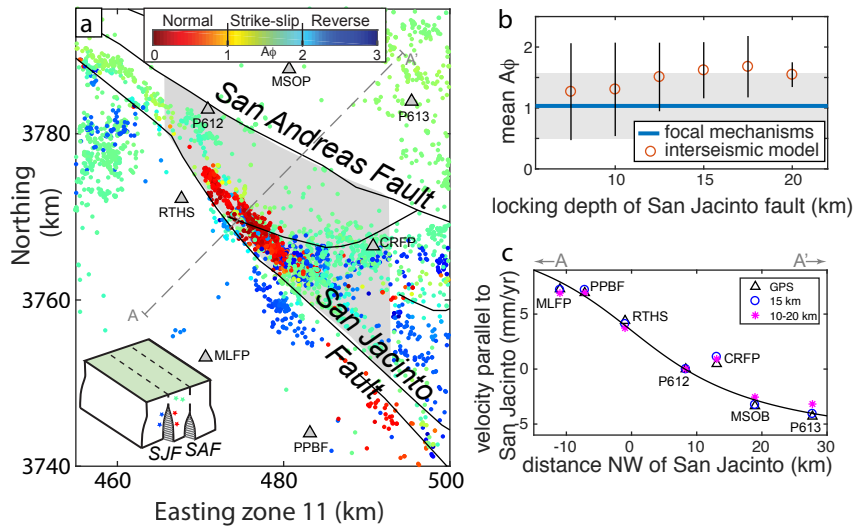


Figure 5. a) Slip sense at locations of microseismicity from the interseismic model with shallow locking depth (10 km) on the San Jacinto fault to simulate deep creep. The locking depth on other faults is 20 km. Inset cartoon shows the set-up of the interseismic model. Normal slip events occur within the San Bernardino basin. GPS stations shown with labeled triangles. b) Mean interseismic slip sense for events within light grey region of A shown with 1σ vertical bars. Models with SJf locking depth < 12.5 km better match the mean slip sense of focal mechanisms in the San Bernardino Basin. c) Transect along A-A' (shown in A) of GPS station velocity parallel to the San Jacinto fault (Herbert et al., 2014), and velocity predictions from the interseismic model with a shallow locking depth on the SJf (pink star, same as results shown in a) and interseismic model with a 15 km locking depth on all faults (blue circle). The surface velocities cannot resolve deep slip on the SJf because of its proximity to the SAF.

206 heterogeneities and deformation along secondary faults (e.g. Anderson et al., 2004) that could act
207 to promote interseismic normal slip microseismicity over a wider region. For example, deep
208 creep along strands parallel to the modeled San Jacinto fault would broaden the predicted zone of
209 off-fault normal faulting.

210 Deep creep along the northern San Jacinto fault may impact seismic hazard estimates on
211 this fault. Both the accommodation of slip along the fault and the accommodation of off-fault
212 deformation within the adjacent crust via microseismicity and aseismic pervasive deformation
213 mechanisms may reduce the interseismic loading on the deeper portion of the northern SJf,
214 thereby reducing seismic hazard. We might also expect moderate or large earthquake to nucleate
215 at the transition between creeping and locked portions (Harris, 2017). Shallow sections of the
216 northern SJf may have increased loading due to deep creep and greater potential for large
217 earthquakes.

218 The correlation between the slip sense of focal mechanism in the San Bernardino basin
219 and patterns of off-fault stressing rate from interseismic models with shallow locking depth on
220 the San Jacinto fault suggests that the interseismic microseismicity of the basin records a
221 component of permanent distributed off-fault deformation in the basin. This result is consistent
222 with a recent study of normal slip focal mechanisms along the Anza section of the SJf (Cheng et
223 al., 2018). If the focal mechanisms of the basin were inverted to estimate interseismic stresses on
224 the SJf and SAf, they would predict normal loading contrary to the long-term slip record of these
225 faults. Using microseismicity that records this off-fault deformation may produce erroneous
226 estimates of interseismic fault loading. Within the San Bernardino basin, the errors of focal
227 mechanism inversions for fault stressing rate are compounded by the under-sampling of strike-
228 slip events along the relatively quiet SAf. This study suggests that where faults creep, spatially
229 non-uniform creep rates may produce non-representative off-fault focal mechanisms. This non-
230 representation is similar to that of aftershocks near rupture ends that have different focal
231 mechanisms than the rupture (e.g. Hardebeck, 2014; Oppenheimer, 1990). Hence, where faults
232 exhibit creep at any crustal level, caution should be used in the inversion of nearby focal
233 mechanisms for interseismic fault loading.

234

235 **Acknowledgments, Samples, and Data**

236 This research was supported by the Southern California Earthquake Center (Contribution No.
237 8079). SCEC is funded by NSF Cooperative Agreement EAR-1033462 & USGS Cooperative
238 Agreement G12AC20038. The authors thank Scott Marshall for sharing his Poly3D executable
239 code and many insightful discussions. Model results of slip sense sampled at locations of
240 microseismicity for the interseismic models with various locking depth are available on figshare
241 (Cooke, 2018).

242

243 **References**

244

- 245 Anderson, M., J. Matti, & R. Jachens (2004), Structural model of the San Bernardino basin,
246 California, from analysis of gravity, aeromagnetic, and seismicity data, *Journal of Geophysical*
247 *Research: Solid Earth*, 109(B4), doi:10.1029/2003jb002544.
- 248 Beyer, J. L., M. L. Cooke, & S. T. Marshall (in revision), Sensitivity of deformation to activity
249 along the Mill Creek and Mission Creek strands of the San Andreas fault, *Geosphere special*
250 *issue on Seismotectonics of the San Geronio Pass Region*.
- 251 Cheng, Y., Z. Ross, & Y. Ben-Zion (2018), Diverse volumetric faulting patterns in the San
252 Jacinto fault zone, *Journal of Geophysical Research*.
- 253 Cooke, M. (2018, May 26). modeled slip style at locations of microseismicity within the San
254 Bernardino basin, CA (Version 2). figshare. <https://doi.org/10.6084/m9.figshare.6361022.v2>
- 255 DeMets, C., R. G. Gordon, & D. F. Argus (2010), Geologically current plate motions,
256 *Geophysical Journal International*, 181(1), 1-80, doi:10.1111/j.1365-246X.2009.04491.x.
- 257 Fialko, Y. (2006), Interseismic strain accumulation and the earthquake potential on the southern
258 San Andreas fault system, *Nature*, 441(7096), 968-971, doi:10.1038/nature04797.
- 259 Field, E. H., et al. (2014), Uniform California earthquake rupture forecast, version 3 (UCERF3)-
260 The time - independent model, *Bulletin of the Seismological Society of America*, 104(3), 1122-
261 1180.
- 262 Hardebeck, J. L. (2014), The impact of static stress change, dynamic stress change, and the
263 background stress on aftershock focal mechanisms, *Journal of Geophysical Research: Solid*
264 *Earth*, 119(11), 8239-8266, doi:10.1002/2014JB011533.
- 265 Harris, R. A. (2017), Large earthquakes and creeping faults, *Reviews of Geophysics*, 55(1), 169-
266 198, doi:10.1002/2016rg000539.
- 267 Hauksson, E., W. Yang, & P. M. Shearer (2012), Waveform relocated earthquake catalog for
268 southern California (1981 to June 2011), *Bulletin of the Seismological Society of America*,
269 102(5), 2239-2244.
- 270 Herbert, J. W., M. L. Cooke, & S. T. Marshall (2014), Influence of fault connectivity on slip rates
271 in southern California: Potential impact on discrepancies between geodetic derived and geologic
272 slip rates, *Journal of Geophysical Research: Solid Earth*, 119(3), 2342-2361,
273 doi:10.1002/2013jb010472.
- 274 Johnson, K. M. (2013), Slip rates and off-fault deformation in Southern California inferred from
275 GPS data and models, *Journal of Geophysical Research: Solid Earth*, 118(10), 5643-5664,
276 doi:10.1002/jgrb.50365.
- 277 Loveless, J. P., & B. J. Meade (2011), Stress modulation on the San Andreas fault by interseismic
278 fault system interactions, *Geology*, 39(11), 1035-1038, doi:10.1130/g32215.1.

- 279 Marshall, S. T., M. L. Cooke, & S. E. Owen (2009), Interseismic deformation associated with
280 three-dimensional faults in the greater Los Angeles region, California, *Journal of Geophysical*
281 *Research*, 114(B12), doi:10.1029/2009jb006439.
- 282 McGill, S. F., L. A. Owen, R. J. Weldon, & K. J. Kendrick (2013), Latest Pleistocene and
283 Holocene slip rate for the San Bernardino strand of the San Andreas fault, Plunge Creek,
284 Southern California: Implications for strain partitioning within the southern San Andreas fault
285 system for the last ~35 k.y, *Geological Society of America Bulletin*, 125(1-2), 48-72,
286 doi:10.1130/b30647.1.
- 287 McGill, S. F., J. C. Spinler, J. D. McGill, R. A. Bennett, M. A. Floyd, J. E. Fryxell, & G. J.
288 Funning (2015), Kinematic modeling of fault slip rates using new geodetic velocities from a
289 transect across the Pacific-North America plate boundary through the San Bernardino
290 Mountains, California, *Journal of Geophysical Research: Solid Earth*, 120(4), 2772-2793,
291 doi:10.1002/2014jb011459.
- 292 Onderdonk, N. W., S. F. McGill, & T. K. Rockwell (2015), Short-term variations in slip rate and
293 size of prehistoric earthquakes during the past 2000 years on the northern San Jacinto fault zone,
294 a major plate-boundary structure in southern California, *Lithosphere*, 7(3), 211-234,
295 doi:10.1130/l393.1.
- 296 Oppenheimer, D. H. (1990), Aftershock slip behavior of the 1989 Loma Prieta, California
297 Earthquake, *Geophysical Research Letters*, 17(8), 1199-1202, doi:10.1029/GL017i008p01199.
- 298 Resor, P. G., M. L. Cooke, S. T. Marshall, & E. H. Madden (2018), Influence of Fault Geometry
299 on the Spatial Distribution of Long - Term Slip with Implications for Determining
300 Representative Fault - Slip Rates, *Bulletin of the Seismological Society of America*,
301 doi:10.1785/0120170332.
- 302 Simpson, R. W. (1997), Quantifying Anderson's fault types, *Journal of Geophysical Research:*
303 *Solid Earth*, 102(B8), 17909-17919, doi:10.1029/97jb01274.
- 304 Smith-Konter, B. R., D. T. Sandwell, & P. Shearer (2011), Locking depths estimated from
305 geodesy and seismology along the San Andreas Fault System: Implications for seismic moment
306 release, *Journal of Geophysical Research*, 116(B6), doi:10.1029/2010jb008117.
- 307 Survey, U. S. G. S. a. C. G. (2006), Quaternary fault and fold database for the United States,
308 edited, , USGS web site.
- 309 U.S. Geological Survey and California Geological Survey, 2006, Quaternary fault and fold
310 database for the United States, January 2017, from USGS web site:
311 <http://earthquake.usgs.gov/hazards/qfaults/>.
312
- 313 Wdowinski, S. (2009), Deep creep as a cause for the excess seismicity along the San Jacinto
314 fault, *Nature Geoscience*, 2(12), 882-885, doi:10.1038/ngeo684.

315 Wiemer, S., & M. Wyss (2000), Minimum magnitude of completeness in earthquake catalogs:
 316 Examples from Alaska, the western United States, and Japan, *Bulletin of the Seismological*
 317 *Society of America*, 90(4), 859-869.

318 Yang, W., E. Hauksson, & P. M. Shearer (2012), Computing a Large Refined Catalog of Focal
 319 Mechanisms for Southern California (1981-2010): Temporal Stability of the Style of Faulting,
 320 *Bulletin of the Seismological Society of America*, 102(3), 1179-1194, doi:10.1785/0120110311.

321

322 **Figure Captions**

323 **Figure 1.** a) High quality focal mechanisms (nodal plane uncertainty $< 45^\circ$) from 1981 through
 324 September of 2016 in the relocated catalog of (Hauksson et al., 2012) with traces of faults active
 325 within the last 15 ka (USGS & CGS, 2006). Colors show slip sense with tangent of slip rake
 326 scaled to the 0-3 range of $A\phi$ slip sense (Simpson, 1997). b) Slip sense predicted by interseismic
 327 crustal deformation model of D at locations of the seismic events recorded in the catalog. Traces
 328 of modeled faults shown in black. Insets show histograms of slip sense. The normal slip events
 329 within the San Bernardino basin are not expected from loading between large earthquakes. c).
 330 Basement depth inverted from gravity data shows secondary normal faults that flank the San
 331 Jacinto fault (taken from Anderson et al., 2004). The normal slip focal mechanisms extend
 332 beyond the interpreted graben. d) Model of 63 active faults in the region used to build the steady
 333 state and interseismic models of crustal deformation. The lateral edges of the horizontal crack are
 334 loaded with plate velocities to simulate the regional tectonic loading (taken from Beyer et al., in
 335 revision).

336

337 **Figure 2.** a) Focal mechanisms from Hauksson et al. (2012) within the region of Figure 1. The
 338 average slip sense for moving window of 600 events shown with black line. Warm colors are
 339 normal events, cool colors are reverse events, and green are strike-slip events. b) Magnitude
 340 completeness limit for a moving window of 600 events advanced in 100 event increments shown
 341 in blue. The stepped red line shows the three stages of magnitude completeness during the
 342 record. c) The 3920 events that exceed the three-phased magnitude completeness limit have
 343 mean $A\phi$ of 1.2 ± 0.04 , indicating limited variation in slip sense during the record. (d-e) The log
 344 of frequency demonstrates the completeness of the catalog for each epoch: 1981 through 2001
 345 (d), 2002 through 2011 (e) and after 2012 (f). The completeness limit (red dashed line) decreases
 346 in each successive epoch.

347

348 **Figure 3.** a) Map view of reliable focal mechanisms that pass the completeness test colored by
 349 slip sense. Enigmatic normal slip events occur within the San Bernardino basin, between the San
 350 Andreas and San Jacinto faults. Dashed fault traces are the graben bounding normal faults
 351 imaged by Anderson (2004) in Fig. 1c. b) Focal mechanisms of the San Bernardino basin (grey
 352 region of a) projected into a N-S profile. Slip sense color same as in a. The normal slip focal
 353 mechanisms within the San Bernardino basin occur predominantly below 7.5 km depth.

354

355 **Figure 4.** Green arrows show the velocities from the steady state model that simulates many
 356 earthquake cycles. The divergence of this velocity field reveals regions of overall contraction

357 (negative dilation blue) and extension (positive dilation red) due to slip distribution along the
358 faults. Inset cartoon shows the set-up of the steady-state model.

359
360 **Figure 5:** a) Slip sense at locations of microseismicity from the interseismic model with shallow
361 locking depth (10 km) on the San Jacinto fault to simulate deep creep. The locking depth on all
362 other faults is 20 km. Inset cartoon shows the set-up of the interseismic model. Normal slip
363 events occur within the San Bernardino basin. GPS stations shown with labeled triangles. b)
364 Mean interseismic slip sense for events within light grey region of A shown with 1σ vertical
365 bars. Models with SJf locking depth < 12.5 km better match the mean slip sense of focal
366 mechanisms in the San Bernardino Basin. c) Transect along A-A' (shown in A) of GPS station
367 velocity parallel to the San Jacinto fault (Herbert et al., 2014), and velocity predictions from the
368 interseismic model with a shallow locking depth on the SJf (pink star, same as results shown in
369 A) and interseismic model with a 15 km locking depth on all faults (blue circle). The surface
370 velocities cannot resolve deep slip on the SJf because of its proximity to the SAF.